SANDIA REPORT
SAND2006-7539
Unlimited Release
Printed March 2007

High Energy-Density Water: Density Functional Theory Calculations of Structure and Electrical Conductivity

Thomas R. Mattsson and Michael P. Desjarlais

Prepared by
Sandia National Laboratories
Albuquerque, New Mexico 87185 and Livermore, California 94550

Sandia is a multiprogram laboratory operated by Sandia Corporation,
a Lockheed Martin Company, for the United States Department of Energy's
National Nuclear Security Administration under Contract DE-AC04-94AL85000.

Issued by Sandia National Laboratories, operated for the United States Department of Energy by Sandia Corporation.

Available to DOE and DOE contractors from
U.S. Department of Energy
Office of Scientific and Technical Information
P.O. Box 62
Oak Ridge, TN 37831

Telephone: (865) 576-8401
Facsimile: (865) 576-5728
E-Mail: reports@adonis.osti.gov
Online ordering: http://www.osti.gov/bridge

Available to the public from
U.S. Department of Commerce
National Technical Information Service
5285 Port Royal Rd.
Springfield, VA 22161

Telephone: (800) 553-6847
Facsimile: (703) 605-6900
E-Mail: orders@ntis.fedworld.gov
Online order: http://www.ntis.gov/help/ordermethods.asp?loc=7-4-0#online

SAND2006-7539
Unlimited Release
Printed March 2007

High Energy-Density Water: Density Functional Theory Calculations of Structure and Electrical Conductivity

Thomas R. Mattsson and Michael P. Desjarlais
HEDP Theory
Sandia National Laboratories
P.O. Box 5800
Albuquerque, New Mexico 87185-MS1186

Abstract

Knowledge of the properties of water is essential for correctly describing the physics of shock waves in water as well as the behavior of giant planets. By using finite temperature density functional theory (DFT), we have investigated the structure and electronic conductivity of water across three phase transitions (molecular liquid/ ionic liquid/ super-ionic/ electronic liquid). There is a rapid transition to ionic conduction at 2000 K and 2 g/cm^3 while electronic conduction dominates at temperatures above 6000 K. We predict that the fluid bordering the super-ionic phase is conducting above 4000 K and 100 GPa. Earlier work instead has the super-ionic phase bordering an insulating fluid, with a transition to metallic fluid not until 7000 K and 250 GPa. The tools and expertise developed during the project can be applied to other molecular systems, for example, methane, ammonia, and CH foam. We are now well positioned to treat also complex molecular systems in the HEDP regime of phase-space.

ACKNOWLEDGMENTS

Tom Mehlhorn is gratefully acknowledged for his lasting support of our work on advanced materials models. We would like to thank Larry Warne for discussions on water switches and electrical break down in general. J.D. Johnson, Eric Chisholm, and Joel Kress at Los Alamos National Laboratory are acknowledged for discussions of water EOS and molecular simulations prior to the project. Jeremy Johnson did some of the simulations and analysis during his time as a summer student in 2005. We have enjoyed discussions with Peter Schultz, Kevin Leung, Ann Mattsson, and Susan Rempe on different aspects of the simulations. The calculations were performed on the center 1600 computational resource koopa as well as on the SNL corporate computational clusters ICC, NWCC, and Thunderbird. The SNL HPC staff, in particular Sophia Corwell, is acknowledged for rapid and efficient troubleshooting on the corporate machines.

CONTENTS

FIGURES

TABLES

Nomenclature

DFT	Density Functional Theory
DOS	Density of States
GGA	Generalized Gradient Approximation
KG	Kubo-Greenwood
LDA	Local Density Approximation
LDRD	Laboratory Directed Research and Development program
PBE	Perdew, Burke, Ernzerhof, a type of GGA.
QMD	Quantum Molecular Dynamics
SNL	Sandia National Laboratories

INTRODUCTION

Water is everywhere, from the highest mountain to the deepest abyss of the ocean, from the pulse shaping water switches in the Z-machine to the prodigious interior of Neptune. The properties of water are thus of great scientific interest as well as of direct interest to the Pulsed Power research program at Sandia National Laboratories. The objective of this LDRD project was to investigate the properties of water in the high energy-density physics (HEDP) regime. We set out to determine the structure as well as develop a quantitative understanding of electrical conductivity in water. The main findings were recently published [1] and different parts of the work have been presented at several international conferences and workshops.

Water switches and domains of interest

Simulations of HEDP systems are routinely done using complex radiation-hydrodynamics codes like ALEGRA, HYDRA, LASNEX, or MACH. Common to all simulations is an extensive use of material models, the quality of which directly determines the fidelity of the simulations. Developing high-quality models is thus very important in order to perform macroscopic simulations with confidence. Water switches are used in the pulse-shaping stage of the Z accelerator [2]. As such, they shorten the pulse by accumulating charge, followed by a rapid release of current after break down. During break down water is taken from normal conditions (300 K, 1 g/cm^3) to high energy-density conditions in fractions of ns.

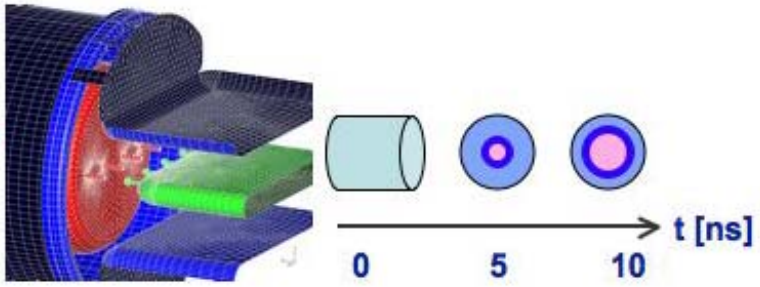

Figure 1. Schematic of a water switch together with an illustration of how the spark creates a plasma channel through the water. Simulated conditions in the channel are drawn in Figure 2.

The phase-space traversed as a spark penetrates the water is shown in Figure 2. The ALEGRA simulations reveals a shock wave moving outwards, compressing the water to 2.5 times normal density and 4000 K. Interior to the shock wave, a channel is formed where the density is low and the temperature rises quickly due to ohmic heating in the plasma. To improve the materials models we have done QMD simulations at selected points in phase-space, the QMD simulations cover a wide range of the phase-space of interest to break down in water. Interestingly, the conditions in the water switch overlap with conditions in the interior of Neptune [3, 4], also shown in Figure 2.

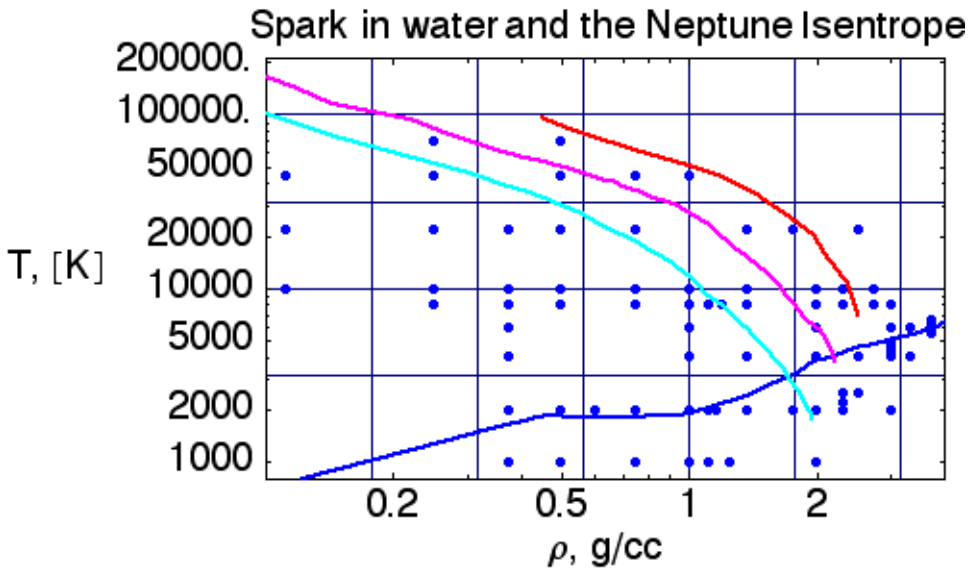

Figure 2. Neptune isentrope (dark blue) [3] and conditions for a spark in water: temperature and densities occurring at different radii away from the center of the channel in an ALEGRA simulation. The three traces are for different times 0.1 ns (red), 1 ns (purple), and 10 ns (light blue). Within 10 ns water exists in conditions between 2.5 times compressed and 10 times expanded density as well between 1000 K and several 100 000 K. Blue dots represents QMD points calculated.

METHOD

The range of temperature, density, and pressure of interest to this problem is significant. With increasing pressure, water goes from an insulating molecular liquid at normal conditions (300K, 1 g/cm^3), to a dissociated ionic fluid, and finally to a dense plasma. We must employ a method that works across several phase transitions; include dissociation of molecules, bound electrons as well as free electrons. The theory must be a quantum theory while at the same time efficient enough to allow for long-time simulations of the dynamics. Density Functional Theory (DFT) has for a long time been successfully been applied to problems in condensed matter physics and chemistry, much more recently DFT has been used in the HEDP regime. DFT combines **Q**uantum level calculations with a speed that enables **M**olecular **D**ynamics simulations, a combination that is often denoted QMD.

Density Functional Theory

DFT is a formally exact reformulation of the Schrödinger equation, the original papers of Hohenberg and Kohn [5] and Kohn and Sham [6] are well worth reading, and so is Kohn's Nobel Lecture [7]. Later reviews are also available, including a recent review by us [8] on the more practical aspects of performing high-quality calculations. The main approximation of the theory is the choice of the so-called exchange-correlation functional. For molecular systems, it is well known that the PBE [9] functional is a better working functional than the Local Density Approximation (LDA) is. For example, the binding energy of a water dimer (the energy of a hydrogen bond, important for liquid structure and diffusion in water) is very accurately reproduced by PBE, with LDA [6] yielding a significantly too high binding energy [10].

Convergence of DFT calculations is of utmost importance. Appendix B describes, in detail, how the water calculations were analyzed in terms of convergence. We have also published an earlier review article dealing with the many aspects of performing well-converged DFT calculations [8].

Kubo-Greenwood response

Michael Desjarlais recently pioneered the use of linear response in the HEDP regime, with the first application being Al [11]. The conductivity of Al in the warm-dense matter regime was successfully investigated using the Kubo-Greenwood (KG) formula for conductivity [11]. The KG formulation gives the conductivity directly from the wave-functions of the system, without assumptions of, for example, relaxation times or cross-sections.

$$\sigma_{\mathbf{k}}(\omega)=\frac{2\pi e^2\hbar^2}{3m^2\omega\Omega}\sum_{\alpha=1}^{3}\sum_{j=1}^{N}\sum_{i=1}^{N}(F(\varepsilon_{i,\mathbf{k}})-F(\varepsilon_{j,\mathbf{k}}))\left|\left\langle\Psi_{j,\mathbf{k}}\left|\nabla_\alpha\right|\Psi_{i,\mathbf{k}}\right\rangle\right|^2\delta(\varepsilon_{j,\mathbf{k}}-\varepsilon_{i,\mathbf{k}}-\hbar\omega)$$

Eq. 1 Kubo-Greenwood conductivity.

.

Here, ε_i is the energy of state i, $F(\varepsilon_i)$ is the Fermi occupation, while $\left\langle\Psi_{j,\mathbf{k}}\left|\nabla_\alpha\right|\Psi_{i,\mathbf{k}}\right\rangle$ is the matrix element for optical transition between states j and i. We have used this approach for studying the electronic properties of water. We find that for water, the electronic contribution to the conductivity begins to be important at 4000 K while above 8000 K, it dominates the conduction for all densities [1].

Ionic conduction/ diffusion

The classical Kubo response formulation is valid for uniform systems where the charged ions are well defined, in that case, the conductivity is given by

$$\sigma=\frac{ne^2}{m}\int_0^\infty\frac{\langle v(\tau)v(0)\rangle}{\langle v(0)v(0)\rangle}d\tau.$$

Eq. 2 Classical Kubo conductivity.

In water, however, the situation is more complex. The initial stage of conduction is dissociation of H_2O into H and OH. After dissociation, protons will move in the water, enabling conduction. A main question is how to calculate the conductivity in this transition phase, where only a few protons contribute to conduction. An additional complication is the diffusive motion itself; protons are not free for a long period of time, but hop between water molecules, it is thus impossible to identify “free” protons and study their diffusion in the long-time limit.

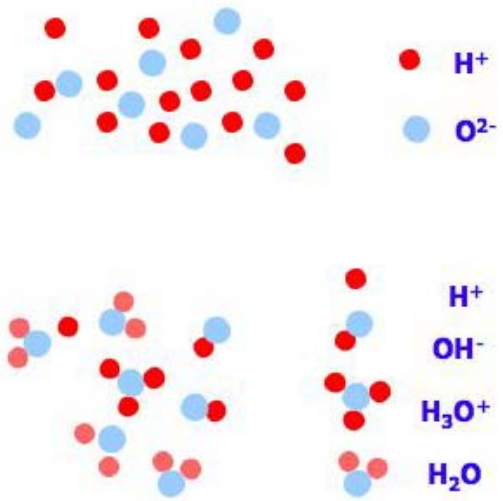

Figure 3. A case of uniform proton conduction (top) and conditions where only a fraction of the protons are conducting (bottom). To be able to model the transition of water from a molecular fluid to dense plasma, it is necessary to also model partial dissociation.

We instead take the partial dissociation into account by analyzing the emerging difference in diffusion between H atoms and O atoms with increased dissociation. In water, H and O are bound, resulting in identical diffusion coefficients for both species. As soon as dissociation occurs, there will be a difference in diffusion between H and O. H atoms will in general diffuse faster than O (H_2O molecules). The diffusion coefficients are calculated separately in the simulation for O (D_O) and H (D_H), the total hydrogen diffusion can be separated into diffusion as H_2O (diffusing as O, with D_O) and diffusion as all other species D_{H*}. Assuming that the fraction of H_2O is γ, we can write the following equations for the conducting part of the motion of protons.

$$D_H = (1-\gamma)D_{H^*} + \gamma D_O$$

$$D_{H^*} = \frac{1}{1-\gamma}\left(1-\gamma\frac{D_O}{D_H}\right)D_H$$

Eq. 3 Subtraction of the neutral, H2O, transport of hydrogen.

Following standard procedures [12], the diffusion coefficients are calculated using the velocity-velocity correlation function according to

$$D = \frac{1}{3}\int_0^\infty \langle v(t) \bullet v(0) \rangle dt,$$

Eq. 4 Diffusion from velocity autocorrelation function.

and the Einstein relation

$$2tD = \frac{1}{3}\left\langle \left| r(t) - r(0) \right|^2 \right\rangle.$$

Eq. 5 Diffusion from the Einstein relation.

The diffusion coefficients from the two relations give equivalent results. We mostly use the velocity-velocity formulation of Eq. 4 since correlation times are relatively short in the HEPD region and since the Fourier transform of the velocity autocorrelation function also yields

information regarding the dynamic properties. We calculate the diffusion coefficient for different end times and verify convergence of the integration of Eq. 4. For low temperatures (2000 K) where the correlation time is long, averaging over up to 15 ps has been necessary. At higher temperatures (6000 – 8000 K) correlation is lost relatively fast and converged values for conductivity are obtained already after 3-5 ps of simulation time.

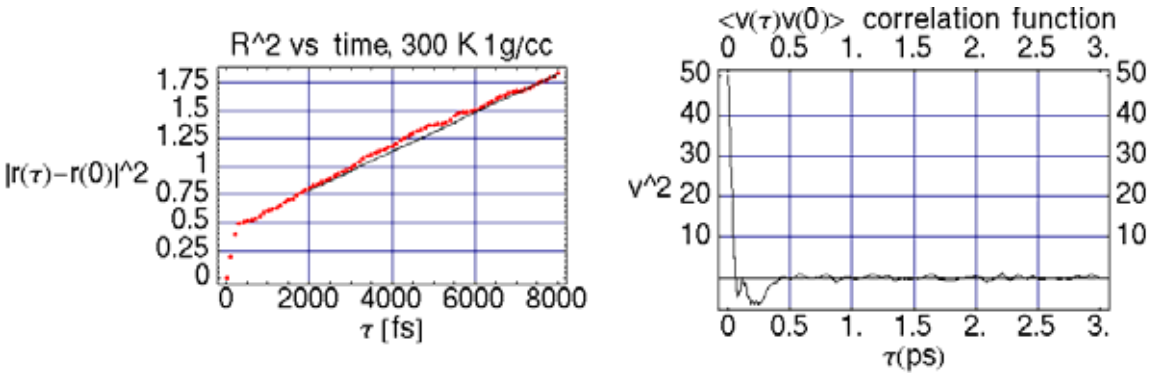

Figure 4. Left: Calculation of diffusion coefficient using the Einstein relation. The straight line is fitted to the long-time behavior and the slope yields the diffusion coefficient. Right: Velocity autocorrelation function, the unit of v^2 is $(A/fs)^2 \times 10^{-6}$. Integration of the correlation gives the diffusion. Note that there is no correlation after 1 ps.

RESULTS

The three main areas of investigation were structure/phase diagram, equation of state ($P(\rho,T)$), and DC electrical conductivity ($\sigma(\rho,T)$). We have studied water between 300 K and 70 000 K, between 0.1 g/cm^3 and 5 g/cm^3.

Phase diagram in the HEPD region

Water has a fascinating phase-diagram, in addition to the on earth naturally occurring hexagonal ice (I_h), liquid, and vapor, water has a number of solid phases: cubic ice I_c, Ice II, III, IV, V, VI, VII, VIII, X, and ice XI. The solid high-pressure phases of water persists until approximately 1000 K. In this work, we have studied water above 1000 K; we will thus not discuss the high-pressure phases of ice. Although not as intricate as the solid ices, the HEDP region has it's own complexity, as evident from the phase diagram of Figure 5. For each QMD simulation, the phase was determined according to the criteria in Table 1. In comparison with earlier work, we propose a revision of the phase-diagram above 3000 K and 500 kBar. The revision is not without consequences since the Neptune isentrope traverses the revised area region of the phase-diagram [3,4]. The full implications of the revision will have to be determined by planetary scientists. However, the existence of interior water with an electrical conductivity of 10^4 1/(Ωm) is likely to affect modeling of, for example, the magnetic fields and electromagnetic energy density of the planet.

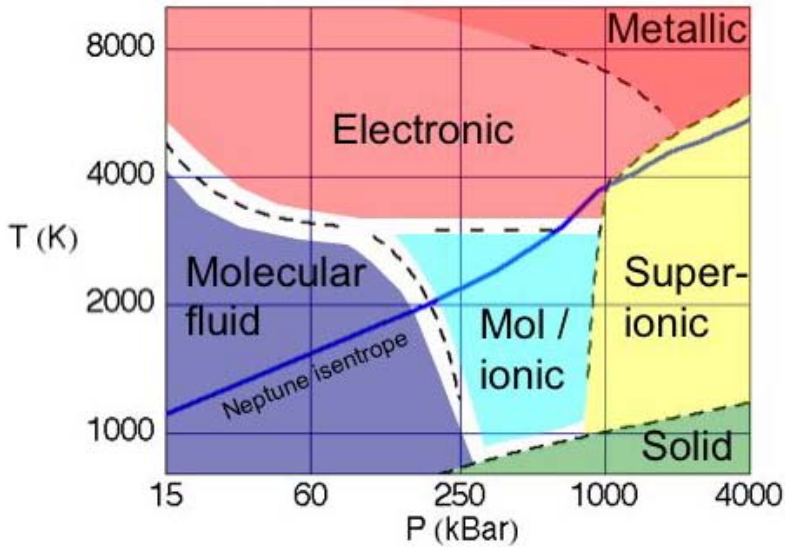

Figure 5. Calculated phase diagram of water in the HEDP region. Our work revises the diagram above 3000 K and 500 kBar, a revision that is not without consequences since the Neptune isentrope [3] traverses that region.

Table 1. Characteristics of the HEDP phases of water in Figure 5.

Phase	Characteristics
Molecular fluid	All H_2O molecules remain un-dissociated during the entire simulation. Gap in the electronic structure, an insulating phase.
Molecular/ionic	Dissociation of water molecules, resulting in a H2O, H, OH, and H3O being present in equilibrium concentrations. The phase ranges from Ionic conduction due to the charged ions. Gap in the electronic structure, an electrically insulating phase.
Super-ionic	O atoms display very little motion, effectively frozen into a lattice. Hydrogen atoms are highly mobile. Ionic conductor due to the fast moving protons. Gap in the electronic structure, an electrically insulating phase.
Electronic	A fluid where O atoms and H atoms both diffuse, an ionic conductor due to the charges ions. Electronic conduction due to partially occupied electronic bands.
Metallic	A fluid where the electrical conductivity is more than 10^5 1/(Ωm). O atoms and H atoms are mobile.

Equation of state: P(ρ,T)

The equation of state for water (as superheated steam) above the critical point (647K) is very well known due to the importance of steam in power cycles. The current state-of the art EOS, based on experimental data, is the one by Wagner and Pruss [13]. The highest tabulated temperature in the article is 1273 K. The SESAME table 7150 [14] is in excellent agreement with WP for 1000K and 1273K, with the 1000 K isotherm, as shown in Figure 1.

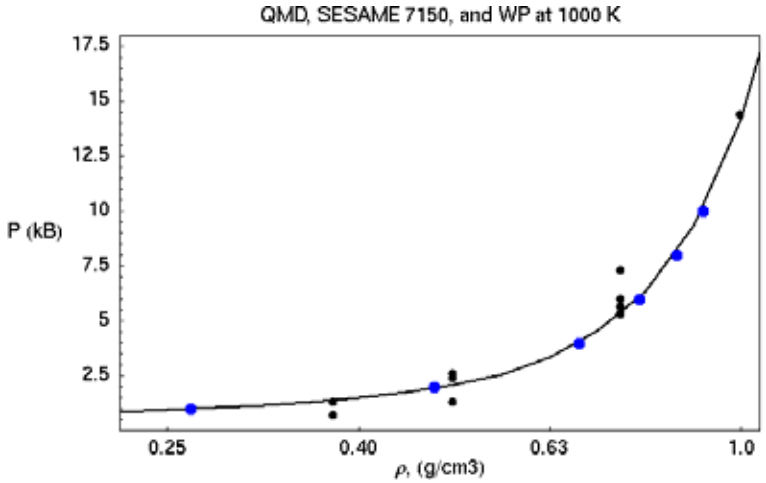

Figure 6. Pressure/density isotherm at 1000K: Wagner-Pruss [13], SESAME 7150 (full black line), and QMD simulations (black points, corresponding to results for different system sizes).

The QMD calculations agree very well with SESAME, and hence the WP EOS at 1000 K. The SESAME table predates WP by 25 years stressing that the properties of the superheated vapor phase of water has been well known for a long time. Through the benchmarking of QMD EOS results at 1000 K, we find that the exchange-correlation functional we currently use (GGA/PBE) is adequate for HEDP systems. This is an important conclusion for H_2O as molecular vapor.

We have performed a large number of calculations to build a QMD database of equation of state for water, calculations ranging from 300 K to 70 000 K, from 0.2 g/cm^3 to 5 g/cm^3. Most points are shown in Figure 7. The calculations are demanding, each EOS point in itself takes of the order 5000 CPU hours. Calculation of electrical conductivity will add 2000-3000 CPU hours, while the most costly calculations are those of diffusion, requiring 20 000 – 40 000 CPU hours.

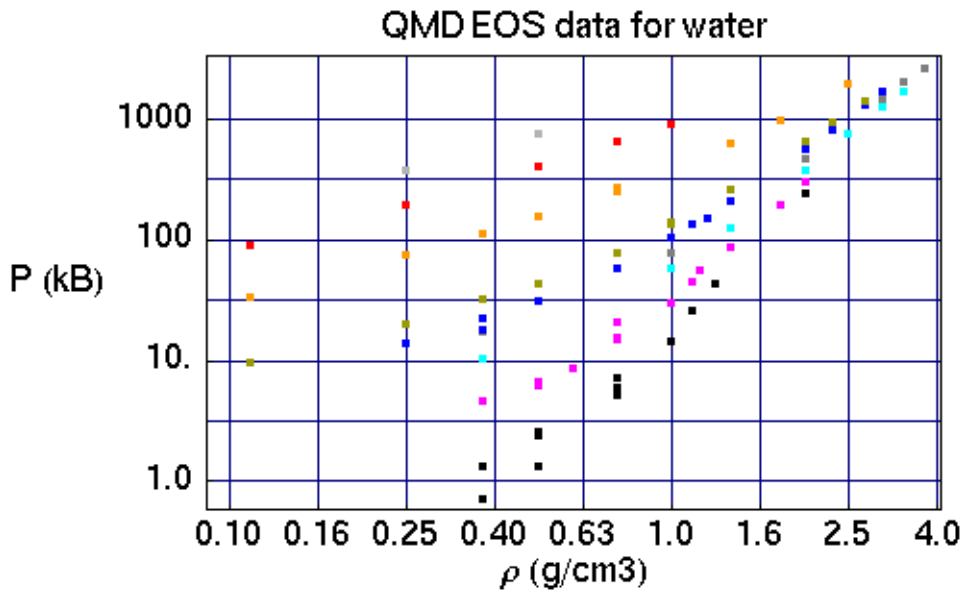

Figure 7. QMD results for equation of state of water, from lower to higher pressure: 1000 K (black), 2000 K (magenta), 4000 K (turqouise), 6000 K (gray). 8000 K (dark blue), 10000 K (green), 22000 K (gold), 44 000 K (red), and 70 000 K (light gray).

With the approach benchmarked with the state of the art EOS (WP), where available, we are confident in the method and will proceed to the regions of phase space of most interest to electrical break down in water switches.

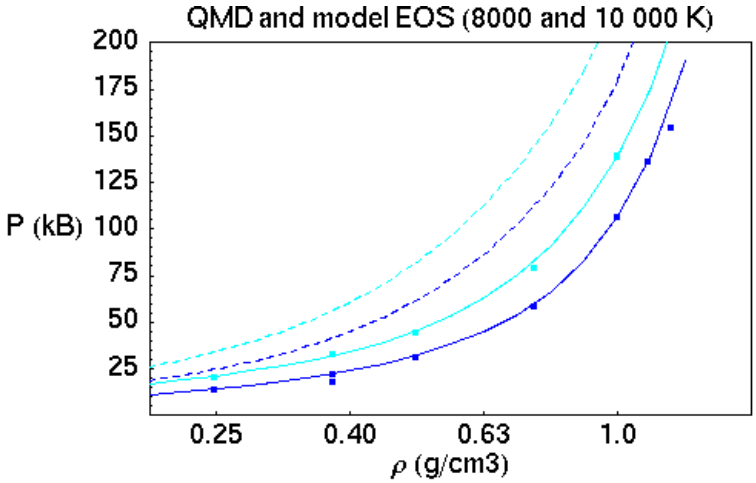

Figure 8. Pressure/density isotherms for SESAME 7150 (dashed), our modified table (full line), and QMD results (points): 8000 K (light blue), 10 000 kK (turquoise). The SESAME EOS overestimates the pressure at intermediate temperatures: the reason being an overestimation of dissociation in this region. Our modified table is fitted to the QMD results, and reproduces them very well.

For increasingly higher temperatures, at first QMD and SESAME pressures deviate more strongly, as shown in Figure 2. The SESAME pressure is too high due to overestimation of dissociation in the regime around 10 000 K. In our simulations at 10 000 K, water is not fully

dissociated whereas the SESAME limiting pressure at low density goes towards a fully dissociated ideal gas.

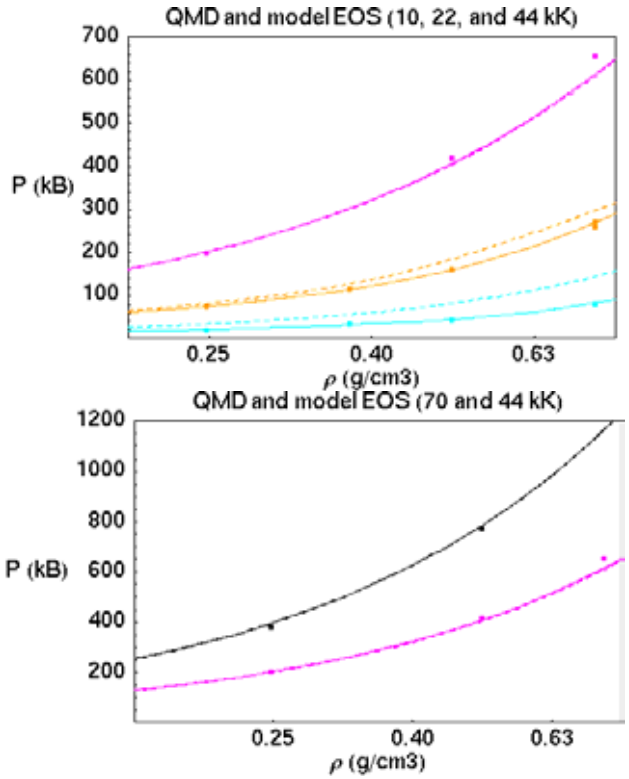

Figure 9. Pressure/density isotherms for SESAME 7150 (dashed), our modified table (full line), and QMD results (points). Left: 10000 K (light blue), 22 0000 K (gold), and 44 000 K (magenta). The SESAME EOS overestimates the pressure at intermediate temperatures, at temperatures where water is fully dissociated the agreement is again very good between the QMD and SESAME pressures.

At higher temperatures, where water is fully dissociated in the QMD simulations, the agreement is again very good. From this behavior, we conclude that modifications of the SESAME EOS are necessary in the region around 10 000 K, while it is sufficiently accurate in the remaining regions investigated. Pressure isotherms between 2000 K and 30 000 K were scaled to agree with the QMD results, the internal energy was subsequently integrated using the thermodynamic identity, and offset using the calculated internal energy from the QMD calculations. The resulting table is a thermodynamically consistent equation of state for water in the difficult regime where dissociation plays an important role.

DC conductivity

The arguably least know property of water in the HEDP regime is the electrical conductivity. Although there exists a qualitative picture, obtained from experiments and some simulations, quantitative data has been scarce over a large region of the phase-diagram. Qualitatively, water, when compressed, will dissociate and transition into a proton conducting ionic fluid. Upon further compression and increased temperature, water becomes an electronic conductor. A main goal of this project was to develop a quantitative picture of the conductivity of water. Figure 10 shows the calculated conductivity over a wide range, both electronic and ionic. At 2000 K, ionic

conductivity dominates over electronic for all densities while the opposite is true above 8000 K. The transition occurs between 4000 K and 6000 K, where the ionic and electronic conductivities are comparable, outside the super-ionic phase. The combined behavior becomes particularly complex at the transition into the super-ionic phase; there, the ionic conductivity continues to increase while the electronic conductivity drops sharply.

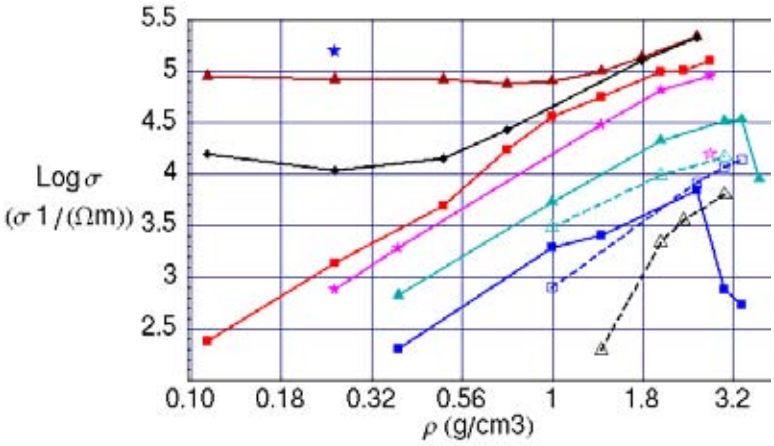

Figure 10. The electronic conductivity (full lines) and ionic conductivity (dashed lines) of water at different temperatures as a function of density. 2000 K (black triangle), 4000 K (blue), 6000 K (turquoise), 8000 K (magenta), 10000 K (red), 22 000 K (black diamond), 44 000 K (brown), and 70 000 K (light blue star).

Electrical conductivity

The electrical conductivity calculated from the Kubo-Greenwood formalism, Eq. 2, is shown in Figure 11. We can identify five different regions of behavior:

A) At 2000 K, and below there is no appreciable electrical conductivity.

B) Beginning at 4000 K, there is significant electronic conductivity over a large range of densities, outside the super-ionic phase.

C) The super-ionic phase of water has a decidedly suppressed conductivity.

D) At 10 000 K, and below, the conductivity falls rapidly with lower density due to localization.

E) Beginning at 22 000 K there is conductivity also at low density, due to ionization and the increased density of states (DOS) for lower density. At 44 000 K the ionization and DOS dominate the conduction, resulting in a weakly varying conductivity with density.

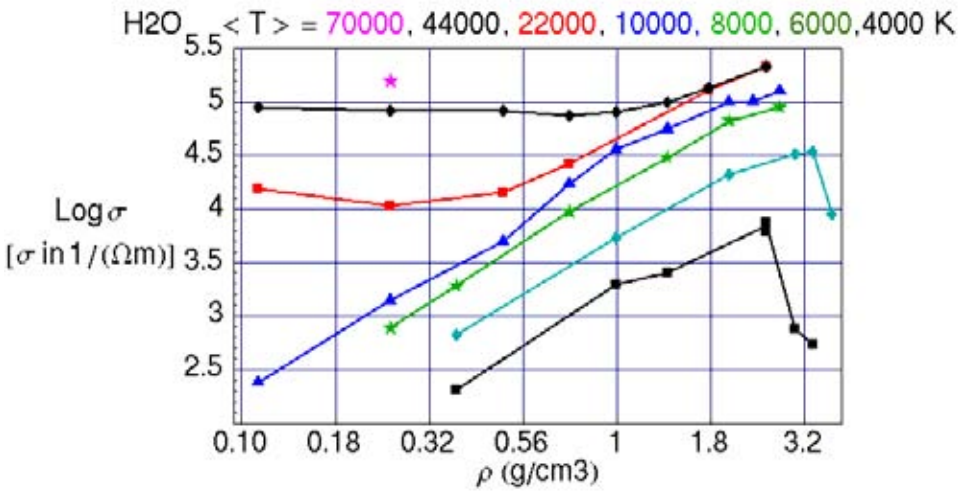

Figure 11 Electrical conductivity for water at different temperatures, ranging from 4000 K to 70 000 K, as color coded in the picture. The sharp drop in conductivity at 4000 K and 6000 K is due to the phase-transition from conducting fluid to super-ionic.

Ionic conductivity

As the density increases, water molecules begin to dissociate, and water turns into an ionic conductor. This transition is rather rapid. As shown in Figure 12, we predict that the ionic conductivity increases more than an order of magnitude when the density is increased from 1.2 to 2.2 g/cm^3. The reduction due to Eq. 1 is important, also shown in Figure 12 is the conductivity if the diffusion coefficient for all hydrogen atoms is included. This is in particular the case for 2000 K, the mobility of water molecules is large enough that interpreting the resulting hydrogen mass transport as conducting will yield a high conductivity also for lower densities, where there is no appreciable dissociation.

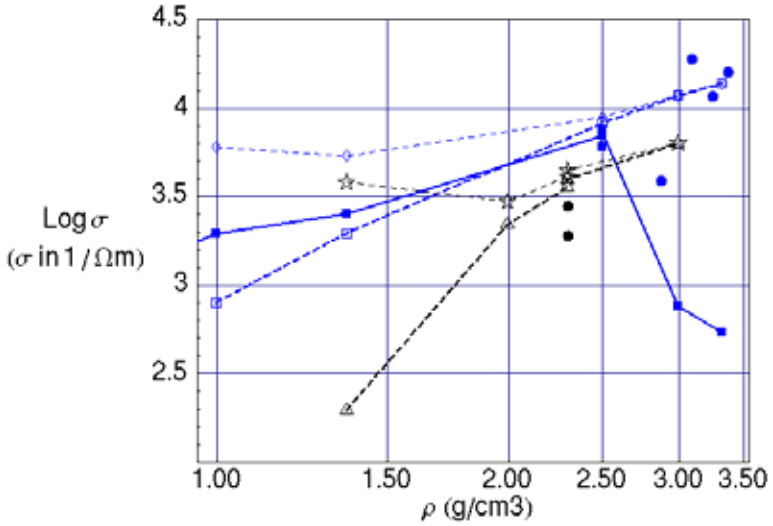

Figure 12. Electronic conductivity at 4000 K (blue solid squares/ blue full line); Ionic conductivity at 4000 K from Eq. 3 (blue open squares/ thick dashed line) and without reducing for neutral diffusion (blue open diamond/thin dashed line); Ionic conductivity at 2000 K from Eq. 3 (black open triangles/ thick dashed line) and without reducing for neutral diffusion (black open star/ thin dashed line). Experimental results for 2000 K [15] (black circles) and between 4000 and 6000 K [16] (blue circles).

CONCLUSIONS

During the project, we have developed a significantly improved understanding of the complex behavior of water. We have revised the phase-diagram in the HEDP region as well as established a quantitative knowledge of the electrical conductivity of water. The tools and expertise advanced during the project can be applied to other molecular systems, for example, methane, ammonia, and CH foam. We are now well positioned to treat also complex molecular systems in the HEDP regime of phase-space.

REFERENCES

1. T.R. Mattsson and M.P. Desjarlais, Phys. Rev. Lett. **97**, 017801 (2006).
2. Larry K. Warne, Roy E. Jorgensen, and Jane M. Lehr, SAND2005-6994 (2005).
3. Nadine Nettelman, private communications and talk at “Physics of Non-Ideal Plasmas”, PNP-12, Darmstadt, Germany (September, 2006).
4. Cavazzoni, et. al. Science **283**, 44 (1999).
5. P. Hohenberg and W. Kohn, Phys. Rev. 136, B864 (1964).
6. W. Kohn and L. J. Sham, Phys. Rev. 140, A1133 (1965).
7. http://nobelprize.org/nobel_prizes/chemistry/laureates/1998/kohn-lecture.html; Nobel Lectures in Chemistry 1996-2000, edited by Ingmar Grethe, World Scientific (2000).
8. A. E. Mattsson et al., Model. Simul. Mater. Sci. Eng. **13**, R 1 (2005).
9. J. P. Perdew, K. Burke, and M. Ernzerhof, Phys. Rev. Lett. **77**, 3865 (1996).
10. X. Xu and W.A. Goddard III, J. Phys. Chem. **108**, 2305 (2004).
11. M. P. Desjarlais, J. D. Kress, and L. A. Collins, Phys. Rev. E **66**, 025401(R) (2002).
12. Allen and Tildesley, *Computer Simulation of Liquids*, Oxford Univ. Press (1988).
13. Wagner and Pruss, J. Phys. Chem. Ref. Data, **31**, No. 2, (2002).
14. SESAME 7150 was constructed at LLNL (1977-78).
15. A. C. Mitchell and W. J. Nellis, J. Chem. Phys. **76**, 6273 (1982).
16. R. Chau et al., J. Chem. Phys. **114**, 1361 (2001).

DISTRIBUTION

Los Alamos National Laboratory

1 Eric Chisholm, Group T-1, MS B221, LANL, P.O. Box 1663, Los Alamos, NM 87545.
1 James D. Johnson, Group T-1, MS B221, LANL, P.O. Box 1663, Los Alamos, NM 87545.
1 Anders Niklasson, Group T-1, MS B221, LANL, P.O. Box 1663, Los Alamos, NM 87545.
1 Joel Kress, Group T-12, MS B268, LANL, P.O. Box 1663, Los Alamos, NM 87545.

Sandia National Laboratories

1	MS0895	Susan Rempe	8333
1	MS1152	Mark Kiefer	1652
1	MS1152	Larry Warne	1652
1	MS1152	Roy Jorgensen	1652
1	MS1168	Clint Hall	1646
1	MS1181	Larry Schneider	1650
1	MS1181	Marcus Knudsen	1646
5	MS1186	Michael Desjarlais	1641
10	MS1186	Thomas Mattsson	1641
1	MS1186	Thomas Mehlhorn	1640
1	MS1190	Keith Matzen	1600
1	MS1191	John Porter	1670
1	MS1322	John Aidun	1435
1	MS1322	Ann Mattsson	1435
1	MS1322	Rick Muller	1435
1	MS1322	Peter Schultz	1435
1	MS1322	Aidan Thompson	1435
1	MS1415	Kevin Leung	1114
2	MS9018	Central Technical Files	8944
2	MS0899	Technical Library	4536
1	MS0123	D. Chavez, LDRD Office	1011

APPENDIX A: PHYSICAL REVIEW LETTERS 97, 017801 (2006)

Phase Diagram and Electrical Conductivity of High Energy-Density Water from Density Functional Theory

Thomas R. Mattsson and Michael P. Desjarlais

HEDP Theory and ICF Target Design, MS 1186, Sandia National Laboratories, Albuquerque, New Mexico 87185-1186, USA

(Received 4 January 2006; published 7 July 2006)

The electrical conductivity and structure of water between 2000–70 000 K and 0.1–3.7 g/cm^3 is studied by finite temperature density functional theory (DFT). Proton conduction is investigated quantitatively by analyzing diffusion, the pair-correlation function, and Wannier center locations, while the electronic conduction is calculated in the Kubo-Greenwood formalism. The conductivity formulation is valid across three phase transitions (molecular liquid, ionic liquid, superionic, electronic liquid). Above 100 GPa the superionic phase directly borders an electronically conducting fluid, not an insulating ionic fluid, as previously concluded. For simulations of high energy-density systems to be quantitative, we conclude that finite temperature DFT should be employed.

DOI: 10.1103/PhysRevLett.97.017801 PACS numbers: 61.20.Ja, 31.15.Ar, 51.50.+v, 62.50.+p

Knowledge of the electronic properties of water is essential for correctly describing the physics of, e.g., giant planets and shock waves in water. The behavior of water is complex due to the dual nature of conduction (ionic and electronic) and an intricate phase diagram. A predicted high-energy-density phase of water [1] was recently confirmed [2,3], adding superionic to the already rich variety of water phases: solid ice (h) to ice XI, liquid, and vapor. Here, we present calculations from first principles of both the ionic and electronic conductivity of water for a wide range of phase space in temperature and pressure, providing quantitative knowledge where little or no previous data are available. The calculations employ a finite temperature Fermi occupation of the electronic states [4], leading to a change in the predicted phase diagram.

Although a qualitative picture of water electrical conductivity has emerged, founded on experiments [5–7] and simulations [1–3,8], much needed quantitative information is scarce. Since experiments can only access certain areas of the phase diagram, and require modeling as a part of the analysis, calculations from first principles arise as a main approach. Density functional theory (DFT) calculations were done with VASP [9], where the Kohn-Sham equations [10] are solved in a plane-wave basis set. Projector augmented wave potentials [11] are used with PBE [12] for exchange or correlation. A Wannier center projection is made for each time step [13]. Most simulations were done using the deuterium mass, reducing computational cost. Both H_2O and D_2O were, however, examined for 2000 K at 2.3 and 3 g/cm^3, yielding a diffusion isotope effect of 1.3, close to the classical $\sqrt{2}$ [14]. A 900 eV plane-wave cutoff energy was chosen to give pressures converged to within 2%. The occupation of bands is set by a Fermi distribution [4]. Our calculations hence differ from the method used in previous studies [1–3,8], where the computationally efficient scheme by Car and Parrinello [15], propagating the electronic degrees of freedom close to the zero-temperature Born-Oppenheimer surface, was used [16,17]. The simulations are in the NVT ensemble using a Nosé thermostat. Pressures, energy, and other properties are calculated as averages after equilibration. The electronic conductivity is calculated using the Kubo-Greenwood formula [18] on 15–20 snapshots from the molecular-dynamics (MD) simulation. About 8 empty bands per water molecule are included in these calculations. Convergence of DFT simulations is of utmost importance [19]. Depending on density and temperature, simulation cells and times vary [20,21]. The gamma point is used for most MD simulations [22] while the mean value point (1/4, 1/4, 1/4) is used for conductivity calculations [21,22]. By a partition of the hydrogen diffusion and a robust method of defining bonds in dense systems, we calculate ionic conduction through the transition from insulating molecular liquid to fully dissociated ionic liquid. The equation of state, ionic conductivities, and electronic conductivities are thus calculated employing a common theoretical platform.

The calculated phase diagram is presented in Fig. 1. With increasing pressure, molecular water dissociates into an ionic liquid, followed by oxygen atoms freezing into the superionic phase. At higher temperature, the fluid is electronically conducting. We find that above 4000 K and 100 GPa, the fluid bordering the superionic phase is conducting. Earlier works instead have the superionic phase bordering an insulating fluid, with a transition to metallic fluid at 7000 K and 250 GPa [1]. This is not a revision without consequences, since the Neptune isentrope [1] is located in this region. The reason for our different result is the finite temperature treatment of the electronic degrees of freedom. By changing the temperature of the Fermi distribution, the electronic structure switches from a metal to an insulator. The effect is documented in Table I and illustrated in Fig. 2. At normal conditions, PBE underestimates the band gap for water

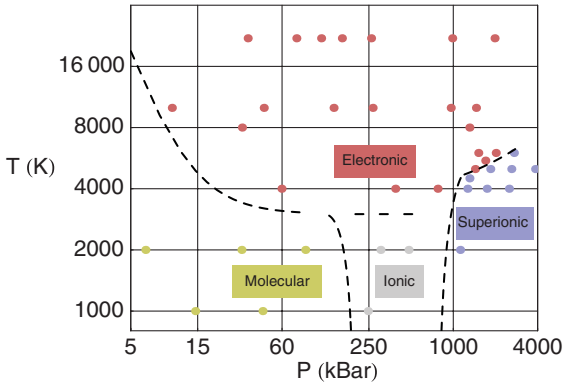

FIG. 1 (color). Theoretical phase diagram for water in the HEDP regime, each point represents a DFT-MD simulation. Molecular liquid—no dissociation of H_2O (yellow). Insulating ionic liquid—dissociation of H_2O and a gap in the electronic structure (gray). Superionic—very small O diffusion coefficient and gap in the electronic structure (blue). Electronically conducting ionic fluid—dissociation of H_2O, no gap in the electronic structure (red). The dashed lines are guides to the eye. The transition from superionic phase to the conducting fluid shows little hysteresis in the phase change, as can be inferred from the dense sampling in that region.

(4.4 vs 6.8 eV). The band closure observed in the simulations, however, is caused by a combination of density, pressure, molecular dissociation, and electronic temperature. It is hence impossible to estimate the true band gap by comparisons to normal conditions. Quantum Monte Carlo (QMC) simulations would provide valuable information, however, QMC is still computationally well beyond reach for this system. The importance of considering the thermal population of electronic states when performing DFT simulations in the high energy-density physics (HEDP) region is a general finding, independent of the outcome of future calculations, or experiments, for this particular system.

TABLE I. Electronic component of the dc conductivity (σ), average occupations (f_i) and energy (ϵ_i) difference $\Delta E = \epsilon_{\mathrm{LU}} - \epsilon_{\mathrm{HO}}$ of highest occupied (HO) and lowest unoccupied (LU) bands (defined when $T_e = 0$) when changing the electronic temperature. Two alternative techniques for smearing, Gaussian and Methfessel-Paxton, both yield gaps. The transition is seen for both 54 and 128 molecules cells. Units are molecules/cell, g/cm^3, Kelvin, $1/(\Omega$ m), occupation, and eV.

n	ρ	T_{ion}	T_e	$\log_{10}(\sigma)$	f_{HO}	f_{LU}	ΔE
54	2.5	4000	1000	0.7	1.98	0.03	1.53
54	2.5	4000	2000	1.2	1.97	0.04	1.74
54	2.5	4000	4000	3.84	1.63	1.25	0.38
128	2.5	4000	4000	3.78	1.63	1.36	0.26
128	2.5	4000	1000	1.0	1.96	0.05	1.01
54	3.0	6000	6000	4.5	1.43	1.25	0.22
54	2.7	8000	8000	5.0	1.28	1.18	0.14

The transition shown in Fig. 2 does not occur instantaneously with a different electronic temperature, it takes of the order 20–100 fs for the new electronic structure to develop, suggesting that reorientation of atoms is required. The transition is seen in the projected local orbital character of the highest occupied state; it changes character from S to P, as seen in Fig. 2. From a computational point of view, the transition time implies that postprocessing snapshots from zero K electronic temperature simulations is not equivalent to a full simulation using finite electronic temperature.

We propose that fast optical diagnostics could be used to investigate this transition, providing information on the electron-ion coupling in H_2O. Shock heating yields hot ions with cold electrons, a state we predict is an insulator. As the system equilibrates through ion/electron scattering, we anticipate a transition to electronic conduction.

Understanding the phase transition from a molecular fluid to a fully dissociated ionic fluid is important for modeling electrical breakdown and other phenomena in shocked water. In this region, a fraction of the hydrogen atoms are dissociated (conducting) while others remain bound as H_2O (nonconducting). Proton diffusion in normal state water occurs via a structural diffusion mechanism involving H^+, OH^-, and H_3O^+ [14,23].

We use Wannier centers (WC) [13,21] to characterize the charge transport. In water at 1000 K/1 g/cm^3, all H atoms are located 0.5 A from a WC; they are bound as H_2O. An *excess* proton, under the same conditions, moves on a path taking it at a distance of 0.75–1.15 A from two or three WCs, simultaneously, before reattaching as a H_3O^+. We find a striking similarity to this behavior in the WC dynamics of the denser systems: H atoms are either bound ($r_{\mathrm{WC-H}} \approx 0.5$) or they are mobile ($0.75 \leq r_{\mathrm{WC-H}} \leq 1.15$

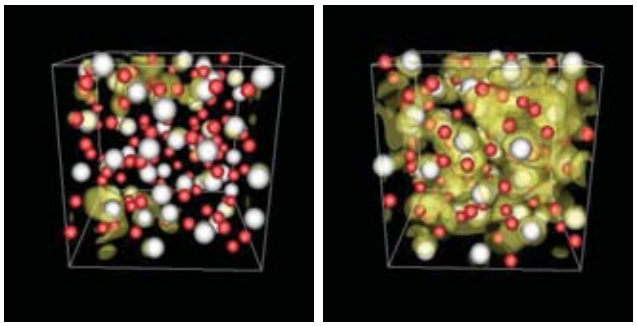

FIG. 2 (color). Snapshots of the structure (oxygen atoms are white, hydrogen atoms red) at $T = 4000$ K and $\rho = 2.5$ g/cm^3. Superimposed is a constant-electron-density surface (gold) projected from the HO state. Using the true temperature induces a shift from S to P character, changing the structure from being localized to spanning the cell, enabling conduction. The shift takes 20–100 fs to appear after changing the electronic temperature from $T_e = 1000$ K to $T_e = 4000$ K. The left snapshot is taken from this transition period, the right snapshot after the system is in equilibrium at $T_e = 4000$ K.

A). Since our findings are consistent with the established proton diffusion mechanism [14,23], we conclude that $+e$ charged protons dominate the conduction also under warm dense conditions.

Instead of analyzing these short-lived complexes, however, we focus on the *nonconducting* hydrogen motion—the transport of hydrogen taking place as H_2O diffusion. The fraction of H atoms bound as H_2O is γ, diffusing with the oxygen diffusion coefficient D_O. With D_H being the diffusion coefficients for *all* hydrogen atoms and D_{H^*} that for all hydrogen species except H_2O, the following relationship holds: $D_H = (1-\gamma)D_{H^*} + \gamma D_O$. Since D_O and D_H are independently calculated in the simulation [24] the conducting part of the mass transport is

$$D_{H^*} = \frac{1}{(1-\gamma)}\left(1 - \gamma\frac{D_O}{D_H}\right)D_H. \quad (1)$$

Although, by construction, D_{H^*} is insensitive to γ [25], we must define "bound". To distinguish scattering from bonds, we consider two atoms bound if they are within a cutoff distance during a time interval. We use the pair-correlation function, with $g(r) = 1$; beyond this point, the concept of bond weakens rapidly. Using the minimum of $g(r)$ has been proposed [3] but the minimum is often flat and leads to very large bonded complexes [26]. Results should not be sensitive to the specific choice of cutoff. Table II shows that it is meaningful to extract the H_2O fraction, γ, in the transition regime between molecular and ionic liquid. Although the ions H^+, OH^-, and H_3O^+ can be considered stable over several fs, the absolute fractions of them depend sensitively on both cutoff criteria, underscoring the difficulty to quantify composition in warm dense systems.

Figure 3 shows calculated conductivity (ionic and electronic) with available experimental data. At 2000 K there is only proton conduction. At 4000 K, the ionic and electronic contributions in the fluid are comparable, while the superionic phase, as expected [1], exhibits a surpressed electronic conductivity. At 6000 K, electronic conduction begins to dominate, and at 8000 K it is an order of magnitude larger than the contribution from protons. Above 22 000 K, water is dissociated and ionization is significant; the increase in density of states for larger specific volume maintains conductivity at low density. Figure 3 displays how Eq. (1) yields a rapid onset of conductivity with increased density due to pressure induced dissociation. Ignoring the nonconducting hydrogen motion results in overestimation of the conductivity. We predict that experiments at 1.5 g/cm^3 will show a very low conductivity. Finally, we note that in the fully dissociated regime there is no difference between the new formulation and the standard relationship between diffusion and conduction.

TABLE II. Distribution of species (mole per mole O) at 2000 K, 2 g/cm^3 when changing the bond cut-off distance, r_{cut}, and steady bond time, τ_{cut}. The fractions used in Eq. (1) are given in bold. The small deviations from neutrality are due to species not included in the table.

τ_{cut}	= **12.5** fs			
r_{cut} (A)	H	OH	H_3O	H_2O
1.10	0.20	0.20	0.012	0.78
1.16	**0.12**	**0.14**	**0.04**	**0.82**
1.20	0.06	0.10	0.06	0.83
1.30	0.006	0.047	0.15	0.81
r_{cut}	= **1.16** A			
τ_{cut} (fs)	H	OH	H_3O	H_2O
10	0.12	0.15	0.04	0.81
20	0.06	0.10	0.06	0.84
45	0.02	0.07	0.07	0.86

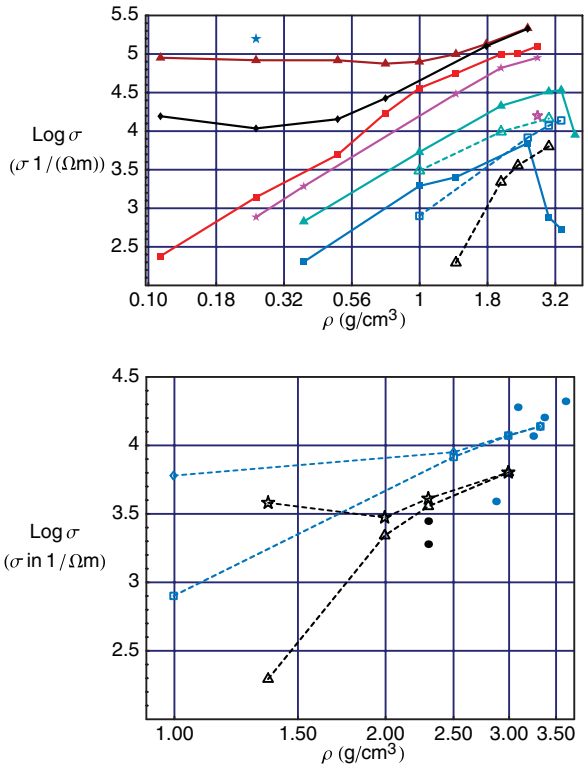

FIG. 3 (color). Upper: electronic conductivity (filled symbols and full lines) and ionic conductivity (open symbols and dashed lines) of water as a function of density for different temperatures: 70 (blue star), 44 (dark red triangles), 22 (black diamonds), 10 (red squares), 8 (magenta stars), 6 (turquiose triangles), 4 (blue squares), and 2 kK (black triangles). The sharp drops in conductivity for 4000 and 6000 K at 2.5 and 3.2 g/cm^3, respectively, corresponds to entering the superionic phase (see Fig. 1.) Lower: Ionic conductivity, as calculated for D_2O and scaled by 1.3 to compare to H_2O experiments. 2000 K from Eq. (1) (black triangles) and using the full hydrogen diffusion (black stars). 4000 K from Eq. (1) (blue squares) and using the full hydrogen diffusion (blue diamonds). Experimental data single shock at approximately 2000 K [5] (black circles) and multiple shock data between 2000 and 6000 K [6] (blue circles).

Recent optical measurements [7] demonstrate a gradual onset of reflectivity along the principal Hugoniot, followed by saturation at $R \approx 0.4$. We find the following reflectivities: 0.1 (4000 K, 2.5 g/cm^3), 0.2 (8000 K, 2.7 g/cm^3), 0.3 (10 000 K, 2.7 g/cm^3), 0.4 (22 000 K, 2.5 g/cm^3), and 0.3 (44 000 K, 1.8 g/cm^3), well in line with the experimental data [7]. Our calculations thus agree with experiments for total conductivity and reflectivity.

In summary, our comprehensive analysis of conduction in water reveals a rapid transition to ionic conduction at 2000 K and 2 g/cm^3, while electronic conduction dominates at temperatures at and above 6000 K. The phase diagram of water is further delineated in the HEDP region, with the superionic phase bordering a conducting fluid above 4000 K and 100 GPa. The resulting increase in electrical conductivity will affect calculations of thermophysical conditions in giant planets as well as how conduction is analyzed in shocked water (electrical breakdown). For first-principles simulations of HEDP systems to be of high fidelity, we show that it is important to include a thermal distribution of the electronic degrees of freedom. We anticipate this work will influence future DFT simulations in the HEDP regime.

We acknowledge fruitful discussions with Peter Schultz and Larry Warne. We thank Tom Mehlhorn for supporting our work and Martijn Marsman for the early opportunity to perform a Wannier center analysis in VASP. The LDRD office at SNL supported this work. Sandia is a multiprogram laboratory operated by Sandia Corporation, a Lockheed Martin Company, for the United States Department of Energy's National Nuclear Security Administration under Contract No. DE-AC04-94AL85000.

[1] C. Cavazzoni, G. L. Chiarotti, S. Scandolo, E. Tosatti, M. Bernasconi, and M. Parrinello, Science **283**, 44 (1999).
[2] A. F. Goncharov *et al.*, Phys. Rev. Lett. **94**, 125508 (2005).
[3] N. Goldman, L. E. Fried, I. Feng, W. Kuo, and C. J. Mundy, Phys. Rev. Lett. **94**, 217801 (2005).
[4] N. D. Mermin, Phys. Rev. **137**, A1441 (1965).
[5] A. C. Mitchell and W. J. Nellis, J. Chem. Phys. **76**, 6273 (1982).
[6] R. Chau *et al.*, J. Chem. Phys. **114**, 1361 (2001).
[7] P. M. Celliers, Phys. Plasmas **11**, L41 (2004).
[8] E. Schwegler, G. Galli, F. Gygi, R. Q. Hood, Phys. Rev. Lett. **87**, 265501 (2001).
[9] G. Kresse and J. Hafner, Phys. Rev. B **47**, R558 (1993); **49**, 14 251 (1994); G. Kresse and J. Furthmüller, Phys. Rev. B **54**, 11 169 (1996).
[10] P. Hohenberg and W. Kohn, Phys. Rev. **136**, B864 (1964); W. Kohn and L. J. Sham, Phys. Rev. **140**, A1133 (1965).
[11] P. E. Blöchl, Phys. Rev. B **50**, 17 953 (1994); G. Kresse and D. Joubert, Phys. Rev. B **59**, 1758 (1999).
[12] J. P. Perdew, K. Burke, and M. Ernzerhof, Phys. Rev. Lett. **77**, 3865 (1996).
[13] I. Souza, N. Marzari, and D. Vanderbilt, Phys. Rev. B. **65**, 035109 (2001); K. Leung and M. Marsman (to be published).
[14] Noam Agmon, Chem. Phys. Lett. **244**, 456 (1995).
[15] R. Car and M. Parrinello, Phys. Rev. Lett. **55**, 2471 (1985).
[16] The Car-Parrinello method has been extended to finite temperature [17], however, no water simulations have been performed, to our knowledge, in that framework.
[17] A. Alavi, J. Kohanoff, M. Parrinello, and D. Frenkel, Phys. Rev. Lett. **73**, 2599 (1994).
[18] M. P. Desjarlais, J. D. Kress, and L. A. Collins, Phys. Rev. E **66**, 025401(R) (2002).
[19] A. E. Mattsson *et al.*, Model. Simul. Mater. Sci. Eng. **13**, R1 (2005).
[20] All shown results for $\rho \geq 1$ g/cm^3 are for 54 molecules. Ten molecules were used for the lowest density $\rho = 0.11$ g/cm^3, 16, and 27 molecules for progressively denser points. Convergence tests were made up to 128 molecules. Simulation times are between 2 and 20 ps depending on the correlation time for each (T, ρ) point. A liquid cell at normal conditions was used as initial structure and the density was changed in steps, followed by equilibration.
[21] See EPAPS Document No. E-PRLTAO-97-036628 for additional information regarding convergence of the density functional theory calculations presented here. It also contains additional information on the Wannier center calculations reported in the Letter and additional references. For more information on EPAPS, see http://www.aip.org/pubservs/epaps.html.
[22] Representative convergence tests were made for both MD and conductivity calculations. The direct superionic/metallic fluid transition was confirmed using a $2 \times 2 \times 2$ k-points mesh for MD. At 4000 K/2.5 g/cm^3 the conductivity changes less than 10% when using 1, 4, 14, and 32 irreducible k points; a finding well in line with our past experience from conductivity calculations of large disordered systems.
[23] D. Marx, M. E. Tuckerman, and M. Parrinello, Nature (London) **397**, 601 (1999).
[24] Diffusion coefficients are calculated using velocity-velocity correlation functions averaged over 5–15 ps, depending on density and pressure. The proton conductivity is calculated using the classic Kubo response formulation using a proton charge of $+e$, as motivated by earlier work [1] and the presented Wannier center analysis.
[25] Proton conduction is primarily manifested in the difference between D_H and D_O. Once a difference exists, whether fewer protons move faster or more protons move slower has little effect on the conductivity.
[26] With $r_{cut} = 1.7$ A at 3 g/cm^3, where the average O-O distance is 2.3 A, H-O bonds are counted well past the nearest oxygen atom, resulting in ''bonded'' complexes like H_4O_2. We focus on finding the fraction of nonconducting H_2O, for which there is no motivation to include anomalously long O-H bonds.

APPENDIX B: EPAPS MATERIAL FOR PHYSICAL REVIEW LETTERS 97, 017801 (2006)

Phase diagram and electrical conductivity of high energy-density water from density functional theory – SUPPLEMENT

Thomas R. Mattsson and Michael P. Desjarlais

HEDP Theory and ICF Target Design,

MS 1186, Sandia National Laboratories,

Albuquerque, NM 87185-1186, USA

(Dated: April 25, 2006)

Abstract

This supplement contains additional information for the letter "Phase diagram and electrical conductivity of high energy-density water from density functional theory". Given the broad scope of the work and the limited space in letter format, we provide a supplement. Here, we demonstrate convergence tests, discuss details of the proton conduction formulation, and summarize the Wannier center analysis.

PACS numbers: 31.15.Ar, 51.50.+v, 61.20.Ja, 62.50.+p

I. INTRODUCTION

The supplement expands the discussion in the Letter in three areas: convergence, proton conductivity derived from a separation of hydrogen diffusion, and the question of charge of the diffusing species. The supplement is not a replacement for a longer paper that will follow, the objective of the supplement is to succintly demonstrate convergence tests and expand the discussion regarding the ionic conduction in water.

II. CONVERGENCE

Convergence of first-principles calculations is of highest importance [1]. We consider the calculations to be very well converged with respect to the relevant parameters. A main purpose of this supplement is to present some of the tests made to ensure that our conclusions are well-founded.

A. Cutoff energy

The simulations reported in the Letter are done with a plane-wave cutoff energy of 900 eV, it was chosen to yield a total pressure converged to 1-2 %, a very strong criterium. Table I and Fig. 1 show the importance of a high enough cutoff energy. Using a cutoff energy that is appropriate for more standard total energy calculations will result in a too low pressure. We also tested different pseudopotentials, no significant difference in pressure was found using the harder 700 eV pseudopotential, the 400 eV PAW PBE potential was used in the simulations.

TABLE I: Total pressure (P_{total}), in kBar, at 4000 K and 2.5 g/cm^3 as a function of cutoff energy (E_{cut}) in eV. The pressure is an average over the last 2 ps of equilibrated simulations. Athough a cutoff energy of 400 eV yields converged total energy differences between structures, it is not enough to calculate the pressure to high accuracy.

E_{cut}	1600	1300	1100	900	700	500	400
P_{total}	784	783	786	780	770	762	688

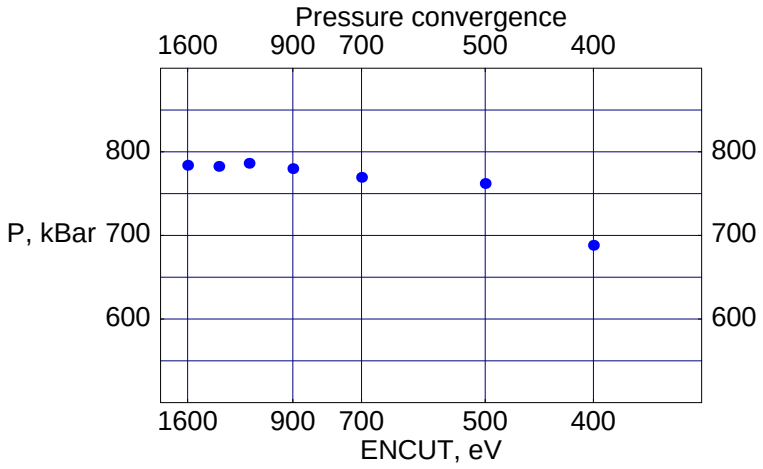

FIG. 1: Convergence of total pressure at 4000 K, 2.5 g/cm^3 with respect to plane-wave cutoff energy. All simulations in the Letter are made with 900 eVcutoff energy, yielding a pressure which is converged to within 2 %.

B. K-points

The gamma point was used for all MD simulations, with occasional tests of multiple k-points. For MD simulations of large disordered cells the gamma point was found adequate. For conductivity calculations, however, it is necessary to go beyond the gamma point. The mean value point (MVP) (1/4, 1/4, 1/4) is used for conductivity calculations. Although a very dense k-point sampling is necessary to give accurate results for conductivity of crystalline solids, this is not the case for highly disordered systems at high temperature. It is our experience from many other materials that the MVP gives sufficiently accurate results. Table II shows that this is a correct assumption also for dense, warm, water. The electronic conductivities in the Letter are for the MVP point. Also note that the conductivity is calculated for 20-30 snapshots from the MD simulation and subsequently averaged.

C. System size

All simulations for densities higher than 1 g/cm^3 reported in the Letter are from cells with 54 or more water molecules, a system size that has been found adequate for water [2], has been regularly used also in the HEDP regime [3, 4], and we confirm to give reliable results. This dense part of the phase-diagram is where the most important new observations

TABLE II: Conductivity as a function of k-point sampling for H_2O at 4000 K and 2.5 g/cm^3. We conclude that using the MVP yields sufficient accuracy. Note that the conductivity is plotted on a logarithmic scale in the Letter. The differences between different k-point sampling can not be detected in a log-plot.

Mesh	# k-pts	σ
MVP	1	0.00699
$2 \times 2 \times 2$	4	0.00758
$3 \times 3 \times 3$	14	0.00728
$4 \times 4 \times 4$	32	0.00720

are made. For regions of phase-space with highly expanded water: densities ranging down to 0.1 g/cm^3, studied at high temperature, and with water more or less fully dissociated, cells with fewer molecules were used (10-16-27). To confirm findings, we performed additional convergence test for system size, up to 128 molecules, for example to verify the behavior of band gap closure with electronic temperature, as reported in Table I of the Letter.

D. MD simulations times

The MD simulation times necessary to gather enough statistics for pressure, energy, and diffusion coefficient are different in different parts of the phase-diagram. The timestep is adjusted and ranges from 0.1 fs to 0.8 fs, depending on temperature and density. For our simulations, we gain maximum efficiency if it takes roughly 4-10 electronic iterations to converge the electronic structure, followed by a force calculation and the atomic MD timestep.

For diffusion calculations, we find that the velocity-velocity correlation function is sensitive to the simulation time, we verified convergence by doing fourier transforms using different end times of the v-v correlation function and varied averaging over the full simulation. Only when the diffusion coefficent was stable with respect to these tests did we terminate the simulation. Diffusion coefficients in the dense region were normally extracted from between 5 and 15 ps of equilibrated simulation.

In the high-temperature, low density regime, the dynamics is fast and nominally "short"

MD simulations required to reach equilibrium. In this regime, we find that snapshots are uniform and accordingly, the variation in electronic conductivity between geometries is small. Note that the timestep per iteration is small in this region due to the fast moving ions, it can be as low as 0.1 fs.

It is our experience that applying a one-size-fits-all approach to cell size and simulations times is not possible with simulations spanning a factor of 35 in density (0.1 - 3.7 g/cm^3) and a factor 70 in temperature (1000 K to 70 000 K). The summarizing statement in the Letter: "Simulation times are between 2 ps and 20 ps" shall be interpreted in this context. Diffusion calculations are not based on 2 ps simulations. Ideal-gas like conditions at high temperature are not simulated for 20 ps.

III. PARTITION OF H DIFFUSION

Using a partition of the hydrogen diffusion, and a robust method of defining bonds in dense systems, we are able to calculate ionic conduction through the transition from insulating molecular liquid to fully dissociated ionic liquid.

We denote the fraction of H atoms bound as H_2O with γ, the diffusion coefficient for oxygen D_O, and the diffusion coefficient for *all* hydrogen atoms D_H. Since hydrogen atoms bound as H_2O diffuse with the oxygen diffusion coefficient, the following relationship holds: $D_H = (1-\gamma)D_{H^*} + \gamma D_O$, where D_{H^*} is the diffusion coefficients for all hydrogen species *except* H_2O. The conducting part of the mass transport is

$$D_{H^*} = \frac{1}{(1-\gamma)} \left(1 - \gamma \frac{D_O}{D_H}\right) D_H. \tag{1}$$

Diffusion coefficients are calculated using the velocity-velocity correlation functions: D_O and D_H are calculated independently of each other as well as independently of γ. The proton conductivity is calculated using the classic Kubo response formulation of conductivity with a proton charge of +e, following the Wannier center analysis presented in Sec. IV, and earlier work [7].

A most important observation is that the ionic conduction of Eq. 1 is not highly sensitive to the estimated fraction of water-bound hydrogen γ. In a molecular fluid, there is no dissociation and $D_O = D_H$, dissociation results in a difference between D_O and D_H. The key aspect of the conductivity is this difference in diffusion between hydrogen and oxygen

atoms. If said difference, in the subsequent step of the analysis, is attributed to slightly fewer or more non-bound hydrogens (for example depending on the definition of γ) is of secondary importance to the resulting conductivity. The effect is demonstrated in Fig. 2 for two temperatures and densities.

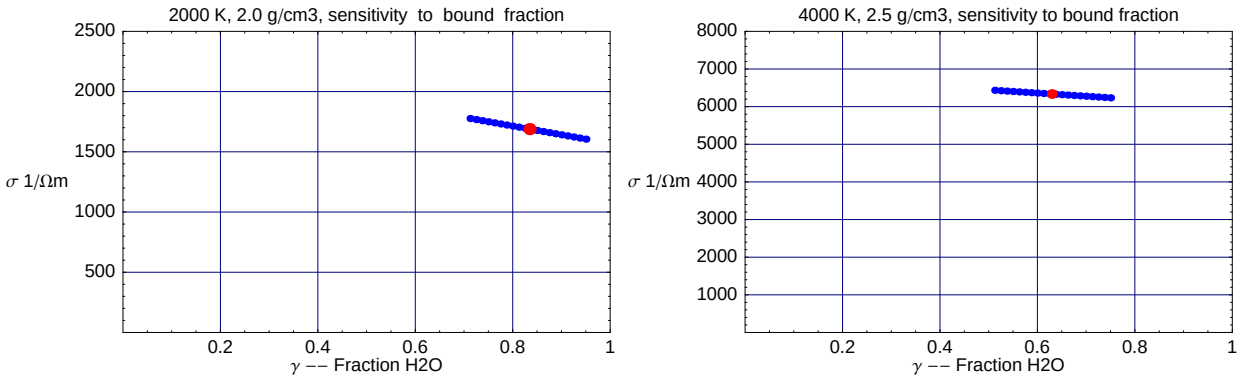

FIG. 2: Proton conductivity resulting from H not bound as H_2O. Using γ obtained from the steady-bond formulation (red, large circle). As a function of γ (blue, small circles). Left: 2000 K and 2.0 g/cm^3, from Table II in the Letter. Right: 4000 K and 2.5 g/cm^3. The proton conductivity is not sensitive to γ.

The sensitivity analysis of γ with respect to cutoff distance and steady bond time (Table II in the Letter) shows that the steady bond analysis determines γ to within 10% in the transition region from molecular water to ionic liquid (2000 K/2 g/cm^3). As shown in Fig. 2, a 10% change in gamma, results in only a small change in proton conductivity. On the Logarithmic scale of Fig. 3 in the Letter, such a change is negligible. Not even a larger uncertainty in γ would cause a significant change in conductivity. Eq. 1 is therefore a very robust formulation of the conductivity.

IV. CHARGE OF H^+

Proton diffusion in water occurs via a structural diffusion mechanism where H^+, OH^-, and H_3O^+ ions, play important roles [8, 9]. In water at normal conditions there is separation of charge: the ions H^+, H_3O^+, and OH^- occur as complexes with well-defined charges. This changes when the system enters the fully dissociated dense plasma limit: ions are screened by free electrons and the effective charge transport by a proton is reduced from +e. Using

the full charge, as done in the Letter, will formally result in an upper bound for the ionic conductivity. In the most intriguing part of phase space, (2000-4000 K, 1 - 3 g/cm^3), however, free protons, free electrons, and free oxygen ions do not dominate the system, there is still substantial molecular structure. Arguably, by studying the motion of hydrogen in time, the structural diffusion process in this regime is similar to the one at lower densities.

To investigate the charge distribution for proton diffusion, we have performed a Wannier Center (WC) analysis [10]. Wannier functions are unitary transformations of the Kohn-Sham eigenfunctions, chosen to be maximally localized in real space. In practice, maximally localized Wannier functions are located at bonds. By comparing the location of the Wannier centers with the location of hydrogen atomic coordinates, we investigate the character of the system. A bound hydrogen atom (OH, H_2O, H_3O) will exhibit one Wannier center located approximately 0.5 A from the atomic coordinate. Calculations on H_2O at conditions well below dissociation show a narrow distribution of distances (r) to the nearest Wannier center, see Fig. 3.

To investigate the behavior of proton diffusion, we added one hydrogen ionic coordinate without adding an electron to the system [11]. The simulation cell consists of 54 water molecules and 1 excess proton. After equilibration, the distribution of distances to nearest WC is very simular to the one in the water cell without the excess proton: the proton mostly occupy an H_3O position. At times, however, the proton hops between water molecules, displaying a brief change in the WC distribution, as shown in Fig. 3. During the hop, the distances to the two nearest WC increases to 0.75 - 1.0 A, with two or more WC located at similar distances. With this analysis of proton diffusion in normal density water, we next proceed to denser systems.

In a dense system with dissociation, the picture changes in a distinct way, as shown in Fig. 4. In addition to the bound hydrogen atoms ($r \approx 0.5$ A), a significant fraction of hydrogen atoms are far away ($r \geq 0.75$ A) from their closest WC, often with two or three WCs at similar distances, the above signature of proton hopping between water molecules. When studying the corresponding hydrogen atoms at the geometrical snapshots in time, we find that these atoms indeed behave as not being bound. They sometimes move rather freely, but more often they are transitioning between neighboring H_2O molecules. The similarity to diffusion of an excess proton in normal density water is striking. We conclude that protons are likely to be responsible for the majority of diffusion also in these denser systems.

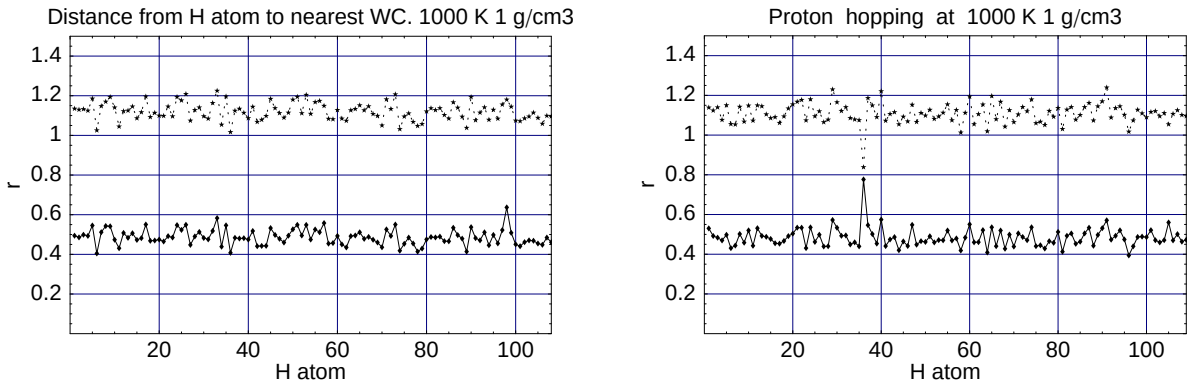

FIG. 3: Left: distance from the hydrogen atomic coordinate to the nearest and next-nearest Wannier centers for water at 1000 K and 1 g/cm^3. There is little variation, all H atoms are bound as H_2O. No dissociation event was ever recorded at these conditions. Right: Signature of hopping event for an excess proton in water at the same conditions (1000 K, 1 g/cm^3), see text.

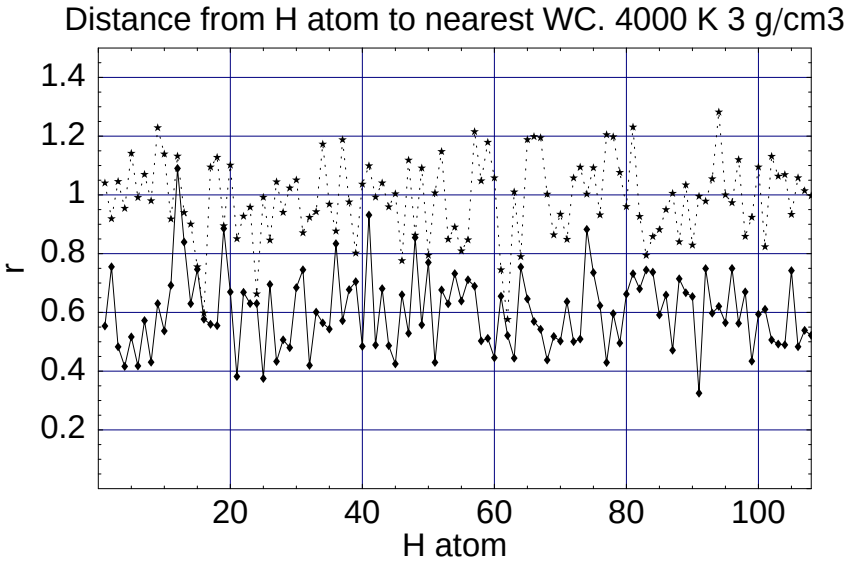

FIG. 4: Distance from the hydrogen atomic coordinate to the nearest and next-nearest Wannier centers at 4000 K and 3.0 g/cm^3. Although most hydrogen atoms are normally bound ($r \approx 0.5$ A) a significant number of hydrogen atoms have their closest WC at a larger distance ($r \geq 0.75$ A).

In addition to this qualitative analysis, we have quantified the distribution of Wannier centers. By averaging the fraction of hydrogen atoms having no WC closer than 0.75 A, and at the same time having a second WC between 0.75 and 1.15 A, we estimate the fraction of

hopping protons in the system. This number comes close to the unbound fraction obtained from the method of counting steady bonds at g(r) = 1.

V. SUMMARY

In this supplement, we have demonstrated convergence test for our calculations, described in detail the partitioning of hydrogen diffusion, and shown how a Wannier center analysis supports the charge of the diffusing proton being +e also in these denser systems.

Acknowledgements

We thank Martijn Marsman for the early opportunity to perform a Wannier center analysis in VASP. Sandia is a multiprogram laboratory operated by Sandia Corporation, a Lockheed Martin Company, for the United States Department of Energy's National Nuclear Security Administration under contract DE-AC04-94AL85000. The LDRD office at SNL supported this work.

---

[1] A. E. Mattsson et. al. Modelling and Simulation in Materials Science and Engineering **13**, R 1 (2005).

[2] J. C. Grossman, E. Schwegler, E. W. Draeger, F. Gygi, and G. Galli, J. Phys. Chem. **120**, 300, (2004).

[3] N. Goldman, L. E. Fried, I.FengW. Kuo, and C. J. Mundy, Phys. Rev. Lett. **94**, 217801 (2005).

[4] E. Schwegler, G. Galli, F. Gygi, R. Q. Hood, Phys. Rev. Lett. **87**, 265501 (2001).

[5] Wagner and Pruss, J. Phys. Chem. Ref. Data, **31** no 2 (2002).

[6] T.R. Mattsson and M.P. Desjarlais, in preparation (2006).

[7] C. Cavazzoni, G .L. Chiarotti, S. Scandolo, E. Tosatti, M. Bernasconi, and M. Parrinello, Science **283** 44 (1999).

[8] Noam Agmon, Chemical Physics Letters **244**, 456 (1995).

[9] D. Marx, M. E. Tuckerman, and M. Parrinello, Nature **397**, 601 (1999).

[10] I. Souza, N. Marzari, and D. Vanderbilt, Phys. Rev. B. **65**, 035109 (2001); C. Berghold, C. J. Mundy, A. H. Romero, J. Hutter, and M. Parrinello, Phys. Rev. B. **61**, 10040 (2000); K. Leung and M. Marsman, to be published (2006).

[11] A uniform background charge maintains charge neutrality.